Materials Science & Engineering C 99 (2019) 255–263

Contents lists available at ScienceDirect

Materials Science & Engineering C

journal homepage: www.elsevier.com/locate/msec

Synergistic antibacterial effects of curcumin modified silver nanoparticles through ROS-mediated pathways

Zhiyong Song[a,1], Yang Wu[a,1], Huajuan Wang[b], Heyou Han[a,b,*]

[a] State Key Laboratory of Agricultural Microbiology, College of Science, Huazhong Agricultural University, Wuhan 430070, PR China
[b] State Key Laboratory of Agricultural Microbiology, College of Food Science and Technology, Huazhong Agricultural University, Wuhan 430070, PR China

ARTICLE INFO

Keywords:
Silver nanoparticle
Curcumin
Nanocomposite
Synergistic antibacterial
Reactive oxygen species

ABSTRACT

Due to their remarkable antibacterial properties, silver nanoparticles (Ag NPs) and curcumin (CCM) have been widely used in the antimicrobial field. In our study, we have fabricated the uniform and stable silver/curcumin composite nanoparticles by a facile ultrasound treatment process and the synergistic antibacterial activity were evaluated. The curcumin not only played a role of reducing agent but also acted as a capping agent. The antibacterial effects of silver/curcumin (cAgNPs) were studied by measuring the growth curve and surface plate assay based on the *E. coli* and *B. subtilis*, which showed concentration dependent bacteriostatic and bactericidal effects of cAgNPs. The presence of CCM enhance the binding of Ag to bacterial membrane and Ag^+ release in comparison to that without CCM, so that creating a temporary and local high Ag^+ concentration near the surface of the bacterium, meanwhile, generation of more reactive oxygen species, lead to membrane damage, bacterial lipases and induce leakage of intracellular contents followed by bacterial death that lead to growth inhibition of the bacteria. The antibacterial effects were characterized by scanning electron microscopy (SEM) and transmission electron microscopy (TEM), the effect which were further found to decrease by introducing antioxidant *N*-acetyl-L-cysteine (NAC) act as a reactive oxygen species (ROS) scavenging agent. These initial data suggest that cAgNPs have a highly antibacterial efficient and might have potential to be developed as an effective antimicrobial nanomaterial.

1. Introduction

Due to the outbreak of infectious diseases caused by different pathogenic bacteria and the exacerbation of antibiotic resistance, exploring new antibacterial agents with favourable safety and strong antibacterial activity that will not engender bacterial resistance are urgently needed [1]. Presently, nanoscale materials, owing to their high surface area to volume ratios and their outstanding chemical and physical properties, have emerged up as novel antimicrobial agents [2]. Different types of antibacterial nanomaterials such as carbon-based nanomaterials [3,4], zinc oxide [5], titanium oxide [6], magnesium [7], gold [8], and silver [9,10] have been developed, but silver nanoparticles (Ag NPs) have proved to be the most effective as they exhibit potential inhibitory and bactericidal efficacy against bacteria, virus and other eukaryotic micro-organisms [10].

The large surface area of Ag NPs allows them to be in better contact with microorganisms and thus, possess good antibacterial ability even at lower concentrations. When Ag NPs enter inside a pathogen, the particle releases silver ions, thereby killing it. Several mechanisms have been proposed to explain the antibacterial activity of silver ion or Ag NPs, such as: the role of surface coating agents [11], generation of reactive oxygen species [12], and released Ag^+ and silver ion stress [13], as well as other fine interactions with bacterial cells [12] that could further trigger downstream damages to the bacterial cell wall via linkages with the respiratory enzymes of bacterial cells [14] or damage DNA, and inhibit DNA duplication [15]. Owing to these properties, nanosilver acts as an effective killing agent against a broad spectrum of (Gram-negative and Gram-positive) bacteria, including the antibiotic resistant strains [10].

There are numerous studies have demonstrated that the bactericidal effect of Ag NPs is closely related with their size [16], shape [17], surface chemistry [18], surface charge [19] and stability [20]. A variety of methods have been developed to synthesize Ag NPs, which include reduction reaction [21], chemical and photochemical reaction [22], thermal decomposition [23], electrochemical process [24], sono-chemical and microwave assisted synthesis respectively [25]. Although

* Corresponding author at: State Key Laboratory of Agricultural Microbiology, College of Science, Huazhong Agricultural University, Wuhan 430070, PR China.
E-mail address: hyhan@mail.hzau.edu.cn (H. Han).
[1] These authors contributed equally.

https://doi.org/10.1016/j.msec.2018.12.053
Received 10 November 2017; Received in revised form 5 June 2018; Accepted 17 December 2018
Available online 19 January 2019
0928-4931/

these methods can successfully produce silver nanoparticles which have different size, shape, surface chemistry and charge in an efficient manner, it usually involves the use of surfactants, reducing agents, and hazardous chemicals which are usually toxic and harmful effects on the environment and human health [26]. Again, the final product requires more purification steps, as some of the chemicals/reducing agents/by-products left behind during the process get adsorbed on the surface of Ag NPs and can cause adverse effects during a medical application or treatment [27]. Additionally, various organic and inorganic substances are added to prevent agglomeration of Ag NPs or control the release of silver ion, which should weaken their antibacterial efficiency [28]. To reduce or eliminate substances hazardous to human health and the environment, identifying and utilizing "green synthesis methods" that correlate in providing higher efficacy of chemical processes are becoming more and more important [29].

Curcumin [(E,E)-1,7-bis(4-hydroxy-3-methoxy-phenyl)-1,6-heptadiene-3,5-ione] is a natural diphenolic yellow orange pigment extracted from the dried rhizome of turmeric *Curcuma longa* [30]. Similar to natural polyphenols, curcumin has possesses a wide range of biological activities, such as antioxidant, antifungal, antibacterial, anti-inflammatory, antiviral effects and so on [31,32]. Recently, it has been shown that curcumin could exert synergistic effect against various bacteria when combined with other agents, including lactoferrin, *N*-acetylcysteine and antibiotics [31]. However, the clinical development of curcumin is severely limited because of its poor solubility in water and low bioavailability [33]. Previous studies have shown that the availability of curcumin in water can be increased by using ultrasound treatment [34], considering that the excellent properties both of curcumin and AgNPs, we expected that curcumin modified AgNPs should have excellent antibacterial activity against bacteria infection.

In our previous work, we reported GO-Silver Nanocomposite as novel antibacterial agents that prevention of pathogenic fungal or bacterial infections in crop protection [3]. In order to simplified preparation process and enhance the biocompatibility, in this work, silver/curcumin composite nanoparticles (cAgNPs) were successfully synthesized by the ultrasound method, as shown in Scheme 1. In this approach, the curcumin not only played a role of reducing agent but also acted as a capping agent. The typical bacterium, *Escherichia coli* (*E. coli*) and *Bacillus subtilis* (*B. subtilis*) were chose to evaluate the antibacterial activity. These results showed that the composites have a much stronger ability to kill bacteria at low concentrations, and the antibacterial mechanism of the silver/curcumin composites was proposed.

2. Materials and methods

2.1. Materials

Curcumin (CCM) and $AgNO_3$ products were purchased from Sinopharm. Propidium iodide (PI) and 4′-6-diamidino-2-phenylindole (DAPI) products were purchased from Aladdin Industrial Corporation of shanghai. Superoxide detection kit and Reactive oxygen test kit were purchased from Beyotime Biotechnology of shanghai.

2.2. Synthesis of cAgNPs and PVP-AgNPs

Curcumin-modified silver nanoparticles (cAgNPs) were prepared via a facile ultrasonic method at room temperature. Briefly, 7 mg curcumin in 10 mL centrifuge tube and add a small amount of ethanol dissolved, then add 2 mL 20 mM sodium hydroxide solution, adjusted to 10 mL with deionized water. And then, 3 mL curcumin was added dropwise to 40 mL of 0.05 mM of silver nitrate solution and ultrasonic for 30 min until the solution from blood red to yellowish green. Subsequently, the resulting product were collected by centrifugation, washed with deionized water, and dried at room temperature.

Synthesis of PVP-modified silver nanoparticles (PVP-AgNPs). First, the silver ammonia solution was dispensed and ammonia was slowly added dropwise to 1 mL, 0.12 mol/L of silver nitrate solution until the precipitate disappeared. Then 0.5 g of PVP was added to 100 mL of a three-necked flask was added 50 mL of ethanol, then heated to 85 °C and refluxed. The prepared silver ammonia solution was diluted 10 times and added to the ethanol reflux system for 2 h. The solution changed from colourless to red. After completion of the reaction, centrifugation was carried out at 10,000 rpm and washed with water and ethanol, respectively, and dried at room temperature.

2.3. Characterization

The UV–vis absorption spectra of the cAgNPs, PVP-AgNPs and CCM were monitored by a spectrophotometer. The particle size was determined by transmission electron microscopy (TEM) spectroscopy on a high-resolution field emission transmission electron microscopy (HRTEM, JEOL Model JEM-2100F). The crystalline structures were characterized by X-ray diffraction (XRD) analysis on a Shimadzu model RX-III X-ray diffractometer (Rigaku, Japan). The hydrodynamic diameter and zeta potentials of the cAgNPs were measured using Nano-ZS ZEN3600 (Malvern Instruments, Malvern, UK). Fourier transform

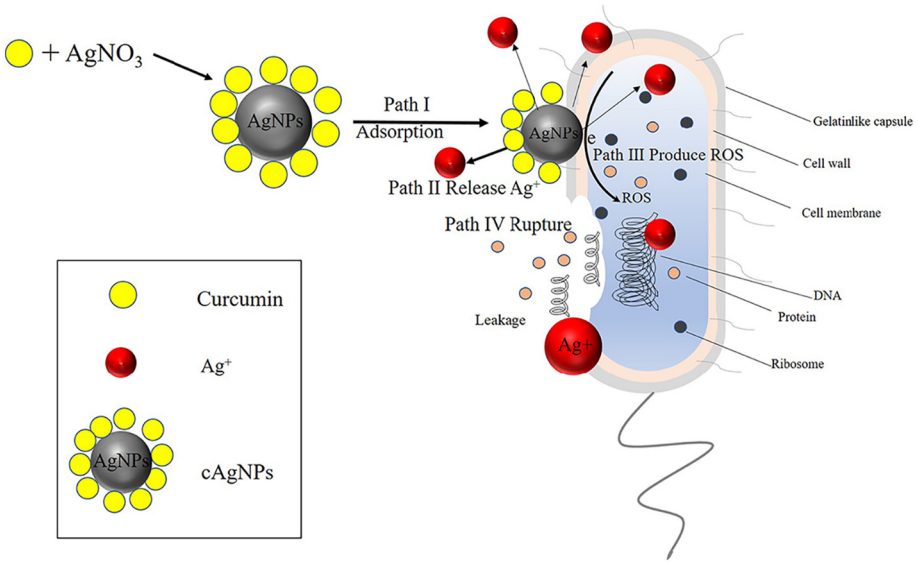

Scheme 1. Schematic diagram illustrating the fabrication and bactericidal process of cAgNPs as a kind of synergistic antibacterial agents.

infrared spectroscopy (FT-IR) studies were carried out using a Shimadzu FTIR spectrophotometer (FTIR 8400).

2.4. Antimicrobial studies

2.4.1. Bacteria culture

Gram-negative *Escherichia coli* (*E. coli*) (AB 93154) and Gram-positive *Bacillus subtilis* (*B. subtilis*) (AB 90008) were acquired from China Center for Type Culture Collection. *E. coli* cells and *B. subtilis* cells were cultivated in Luria-Bertani nutrient solution (LB), followed by incubation in a rotary shaker at 120 rpm and 30 °C for 12 h. After that, the bacterial cells were harvested by centrifugation at 3000 rpm for 3 min, then the cells were resuspended in water, and the final cell density was adjusted to about 1×10^8 colony forming unit (CFU)/mL. All solid/liquid materials had been autoclaved for 30 min at 121 °C before use.

2.4.2. Antibacterial tests

The antimicrobial activity was evaluated by surface plate, antibacterial ratio, and growth curves. Two types of bacterial, *E. coli* and *B. subtilis*, were used. The detail procedure of the surface plate test and optical density (OD600) were as following: 200 μL cell suspension and 200 μL cAgNPs, PVP-AgNPs and CCM with different concentration were mixed and incubated in a rotary shaker at 120 rpm for 3 h at 30 °C. Control samples contained 200 μL of the cells suspension mixed with 200 μL of deionized water. Each group was divided into two tubes, one tube was used to surface plate test, the other was used to growth curves test. After 3 h treatment, 10 μL of mixtures liquid was taken out for dilution with LB media 10,000 times. Afterward, the number of colonies was counted after culturing, the culture time was 12 h for *E. coli* and 24 h for *S. aureus* at 30 °C, respectively. By counting the number of colonies on the plate, one can calculate the antibacterial rate. The antibacterial ratio was calculated using the following formula:

$$\text{Antibacterial rate } (\%) = \left(1 - \frac{\text{CFU(expermental group)}}{\text{CFU(control group)}}\right) * 100\%.$$

The other tube mixtures were transferred into 20 mL LB broth. The *E. coli* cells and *B. subtilis* samples were then incubated at 30 °C in an incubator with constant agitation at 120 rpm. Growth rates and bacterial concentrations were investigated under varying concentrations cAgNPs, PVP-AgNPs and CCM materials by measuring the OD600 every 1 h.

To observe the morphological changes of bacteria before and after exposure to cAgNPs, PVP-AgNPs and CCM materials in medium, the bacteria were cultured through the aforementioned process, the structure of bacteria were observed using TEM and SEM. The treated bacteria were centrifuged at 6000 rpm and fixed by 2.5% glutaraldehyde for 4 h and then dehydrated with 30%, 50%, 70%, 90% and 100% ethanol for 15 min each time, respectively. Next, the treated sample was freeze-dried. Finally, the thin sections containing the cells were mounted on copper grids for SEM and TEM examination.

2.4.3. Fluorescence imaging

In order to more intuitive performance of the bacteria on the bactericidal effect, we use propidium iodide (PI) and 4′-6-diamidino-2-phenylindole (DAPI) after the materials treatment of the suction was stained. They were stained with PI (100 μg/mL) and DAPI for 15 min and 5 min in the dark, respectively. Fluorescence images were taken on an Olympus BX40 fluorescence microscope during a single batch experiment at 400× magnification.

2.4.4. Intracellular components leaked protein

The leakage of intracellular compounds reflects the permeability of the cell membrane and cell wall. The BCA protein assay kit (Beyotime, Shanghai) was used to determine the extracellular protein concentration of the bacteria suspension and the detailed process could be found elsewhere. 20 μL of the treated bacterial solution was added to the 96-well plate, and then 200 μL of the protein working solution was added to each well plate and incubated at 37 °C for 20–30 min. OD590 were monitored to quantitatively determine the leaked protein.

2.5. Effect of oxygen and antioxidants on the antibacterial activity of AgNPs

2.5.1. Intracellular ROS level evaluation

The intracellular reactive oxygen species (ROS) level was investigated by fluorescence imaging. The samples were washed with PBS twice after treatment by materials and then 100 μL of 20′,7′-dichlorodihydrofluorescein diacetate (DCFH-DA, Beyotime, China) were added to the surface and reacted for 15 min. The excess dye was washed with phosphate buffer saline (PBS) and the samples were observed by inverted fluorescent microscopy as mentioned above.

The superoxide levels were measured via employing superoxide assay kit (Beyotime Biotechnology) according to the manufacture's protocol. Briefly, 200 μL bacterial suspension was centrifuged and washed twice with sterile water, followed by adding 200 μL superoxide detection solution and incubated at 37 °C for 5–10 min. Then, adding different concentrations of BQAS and incubating with the same conditions as before. After incubation, the result was examined by microplate absorbance reader at 450 nm.

2.5.2. Antioxidants on the antibacterial activity of AgNPs

The antioxidant *N*-acetyl-L-cysteine (NAC) was used to investigate the effect of reactive oxygen species (ROS) on the antibacterial activity of cAgNPs. To do this, two sets of culture, one with cAgNPs alone and another with cAgNPs and NAC (0.1 mM) were prepared containing different concentrations cAgNPs. A control containing 0.1 mM NAC in the presence of *E. coli* or *B. subtilis* alone under similar conditions was used to establish the effect of NAC in the absence of cAgNPs.

2.6. Ag ion release test

The concentration of released Ag^+ was also determined. 200 μg/mL of cAgNPs and 100 μg/mL of PVP-AgNPs were placed, and the solution was uniformly dispersed in 20 mL of LB medium and dispensed into a 2 mL centrifuge tube. Then the solution was incubated at 30 °C and takes a sample every 12 h. The mixture was centrifuged at 10,000 rpm for 10 min, and the supernatant filtered through a 0.22 μm membrane so that the nanoparticles were removed as pellets while Ag^+ remained in the supernatant. The concentration of Ag^+ in the solutions was determined by inductively-coupled plasma mass spectroscopy (ICP-MS).

2.7. Statistical analysis

Each experiment was repeated at least 3 times and the results were shown as mean ± stand deviation (SD) and analyzed by Student *t*-test and ANOVA test. A value of $P < 0.05$ was considered statistically significant.

3. Results and discussion

3.1. Preparation and characterization of cAgNPs

In this synthesis procedure of cAgNPs nanocomposites, curcumin used as the reducing agent and capping agent of $AgNO_3$ was prepared. Transmission electron microscopy (TEM) showed that the resulting cAgNPs nanoparticles were sphere and had a relatively uniform diameter of 35 ± 5 nm (Fig. 1A), Dynamic light scattering (DLS) measurements showed that the cAgNPs have a hydrodynamic diameter of particles ranged from 30 to 90 nm (Fig. S1A) and a zeta-potential of −27.9 mV (Fig. S1B). The UV–visible spectrum of cAgNPs, PVP-AgNPs and CCM were depicted in Fig. 1B. Curcumin strongly absorbs in the

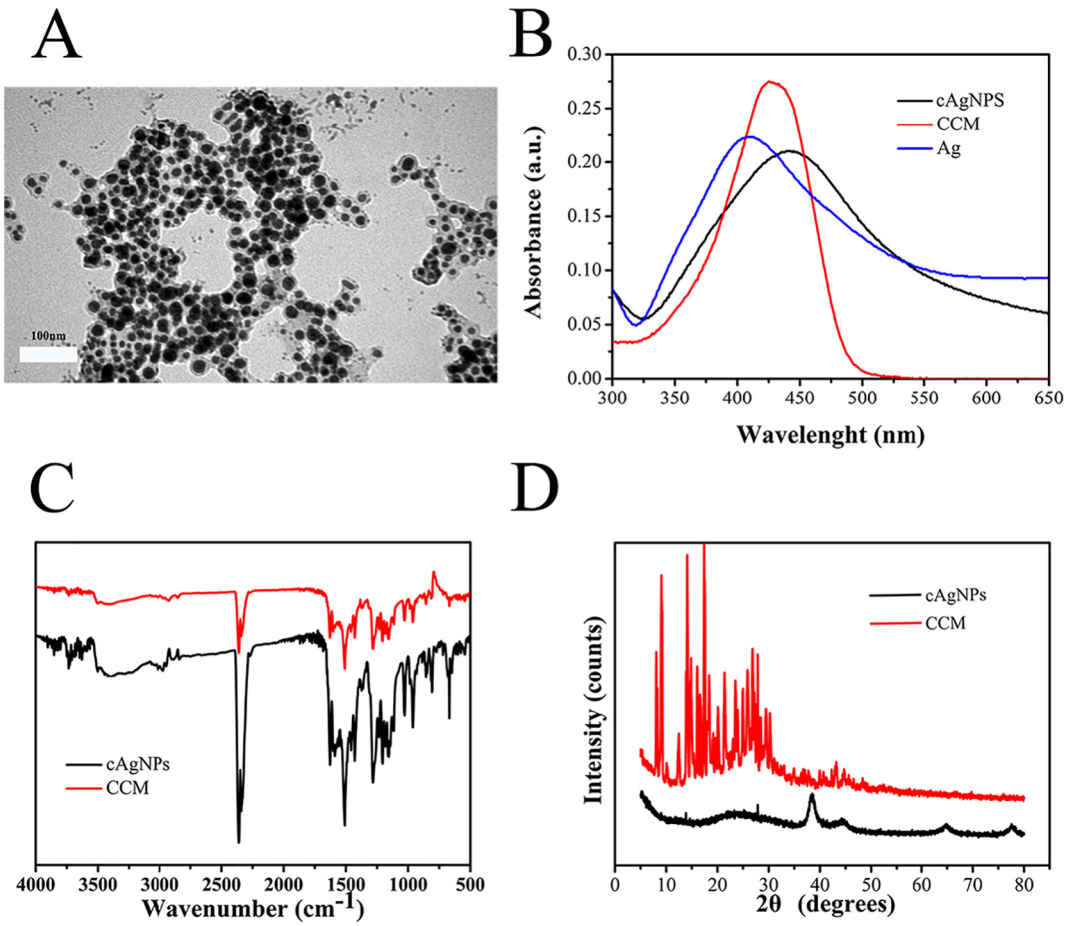

Fig. 1. (A) TEM image of the cAgNPs. (B) UV–vis absorption spectrum of CCM, PVP-AgNPs, cAgNPs. (C) FT-IR of cAgNPs and CCM. (D) XRD pattern of CCM and cAgNPs.

UV–vis region at around 426 nm in aqueous media, characteristic silver plasmon band at 410 nm in the UV–vis region, however, the cAgNPs had a prominent peak at around 439 nm, which indicates a strong association of curcumin with Ag^+. FT-IR analysis was done to further confirm the caging of curcumin onto silver nanoparticles, As Fig. 1C shows, the absorption peaks at 2920 cm^{-1}, the asymmetric C—H stretching of $-OCH_3$ groups, appear either in curcumin or cAgNPs, indicating that the synthetic reaction of cAgNPs does not involve the methoxy groups. On the other hand, the absorption peak at 1627 cm^{-1} in curcumin, owing to a contemporaneous contribution of C═C and C═O stretching mode, while the strong absorption peaks at 1149 cm^{-1} and 1276 cm^{-1}, which was assigned to the enol C—O peak of curcumin. The FTIR data showed that the as-prepared AgNPs were capped with curcumin successfully. X-ray diffraction (XRD) showed that the AgNPs were successfully capped with curcumin per the peak position (Fig. 1D). The amount of Ag^+ that has been incorporated on the nanoparticle was determined by ICP-MS, the results showed that contents of silver and curcumin in cAgNPs were about 50.25% (Table S1).

3.2. Synergetic effects of cAgNPs nanocomposites on inhibiting the bacterial growth

To quantitatively investigate the synergetic antibacterial effects, the survival rates and growth curves of bacteria exposed to cAgNPs, PVP-AgNPs and CCM were measured. *E. coli* and *B. subtilis* were chosen as the Gram-negative and Gram-positive bacteria model respectively in this test. Plant counting method was used to determine the antibacterial ability (Fig. S2). The lower survival rate indicates the lower activity of the bacterium (Fig. 2). Approximately 10^8 CFU mL^{-1} *E. coli* and *B. subtilis* cells were grown in 0.2 mL liquid LB medium supplemented with various concentrations CCM, PVP-AgNPs and cAgNPs nanocomposites. Compared with cells treated by PVP-AgNPs and curcumin, the death rate reached > 95% after being treated with cAgNPs in water (at a concentration range from 12.5 μg/mL to 200 μg/mL), obviously suggesting that the higher the concentration of cAgNPs, the lower the survival rates of bacterial cells. Taner et al. results showed that the AgNPs for antibacterial purposes with a reported MIC of > 150 μg/mL against *E. coli* strain at ~10^8 CFU mL^{-1} initial bacterial concentration [35]. The MICs of the PVP-AgNPs, curcumin (CCM) and cAgNPs against *E. coli* and *B. subtilis* are summarized in Table 1. The cAgNPs display the lower MIC than the PVP-AgNPs, it means that the cAgNPs have better inhibitory activity against the *E. coli* and *B. subtilis*.

To investigate the bacterial inhibitory and killing effects of CCM, PVP-AgNPs and cAgNPs nanocomposites, the growth kinetics of *E. coli* and *B. subtilis* in liquid media were studied (Fig. 3). Bacterial growth was monitored by measuring the optical density at 600 nm (OD600) based on the turbidity of the cell suspension. Obviously, the increased concentrations of cAgNPs nanocomposites lead to the reduced survival rates of bacteria. Pure PVP-AgNPs or CCM was used as a control sample for comparison, and there was no obvious inhibition of the bacterial growth even at a high concentration of 100 μg/mL. However, the growth was inhibited completely by the cAgNPs nanocomposites, indicating that the cAgNPs nanocomposites had excellent antibacterial activity against both Gram-negative *E. coli* and Gram-positive *B. subtilis* in a concentration-dependent manner. More important, cAgNPs nanocomposites exhibited greater inhibitory capability against bacterial proliferation than Pure PVP-AgNPs or CCM at the same dosage concentration, implying that the antibacterial activity was obviously

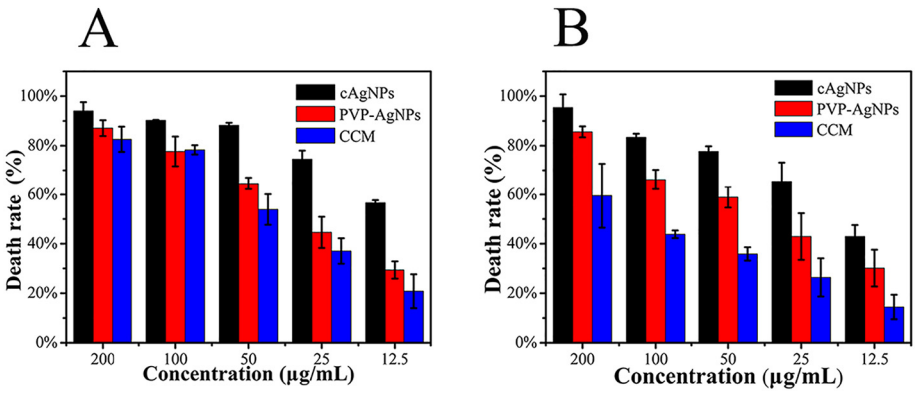

Fig. 2. Cell death rate of (A) *B. subtilis* and (B) *E. coli* bacterial after incubation with cAgNPs, PVP-AgNPs and CCM at different concentration (12.5, 25, 50, 100, 200 μg/mL).

Table 1
Minimal inhibitory concentrations of PVP-AgNPs, curcumin and cAgNPs against *E. coli* and *B. subtilis*.

Bacteria	PVP-AgNPs (μg/mL)	CCM (μg/mL)	cAgNPs (μg/mL)
E. coli	32	64	8
B. subtilis	32	64	8

Note: Studies were done at 10^5 CFU mL^{-1} initial bacterial concentrations.

enhanced when the silver nanoparticle combined with curcumin. Furthermore, potential synergistic antibacterial effects were quantified by the fractional inhibitory concentration (FIC) index, which was determined using minimal inhibitory concentrations (MICs) obtained by the microdilution checkerboard method [36]. The result was presented in the Table 2. The MICs of PVP-AgNPs and of curcumin were reduced from respectively 32 and 64 μg/mL for the agent alone to 8 μg/mL and 16 μg/mL. Combinations of PVP-AgNPs with curcumin (CCM) were highly synergistic against *E. coli* (FIC index = 0.375) and *B. subtilis* (FIC index = 0.5).

To further investigate the antibacterial activity of the cAgNPs to *E. coli* and *B. subtilis* bacterium, fluorescence microscopy was used to examine the survival rate of cells after incubation with cAgNPs dispersions by a Live/Dead bacterial viability kit. DAPI labels live bacteria with blue fluorescence, and propidium iodide (PI) labels membrane-compromised bacteria with red fluorescence. As seen in Fig. 4, there was only weak red fluorescence after treatment with pure CMM or PVP-AgNPs (Fig. 4a2–a4, b2–b4), however, the strong red fluorescence was displayed after treatment with cAgNPs (Fig. 4a1, b1) based assays showed that cells incubated with cAgNPs nanocomposites for 3 h, suggesting that an abundant number of bacteria were dead and the cAgNPs nanocomposites could efficiently kill the bacteria. As we all know, the PI as a cell membrane impermeable fluorescent dye which could only enter into broken cell membranes and showed enhanced fluorescence after binding to nucleic acid [37]. Therefore, these results revealed that cAgNPs nanocomposites possessed efficient ability to disrupt the membrane structure of bacteria. It is not only in good agreement with the result obtained by the CFU method, but also suggests that the cell membrane was damaged. In summary, all these in vitro experiments indicate the cAgNPs nanocomposites have strong antibacterial properties when tested against both Gram-positive and Gram-negative bacteria.

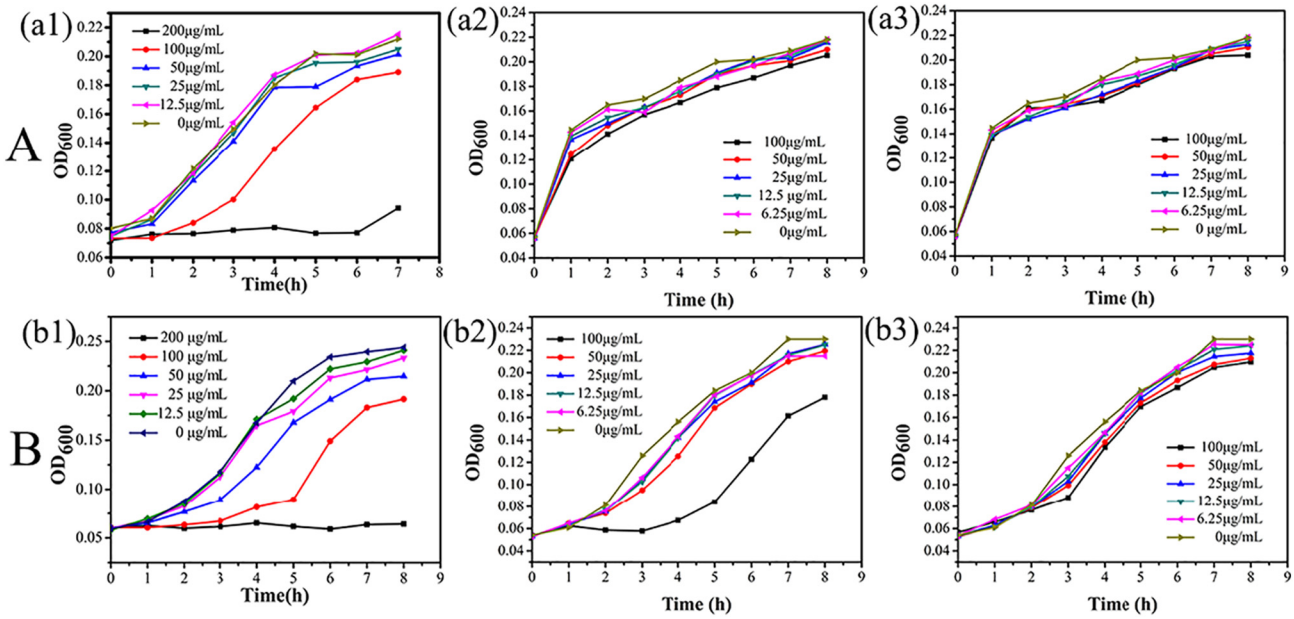

Fig. 3. Growth curves of *B. subtilis* (A) and *E. coli* (B) in LB broth with different concentration of materials treatment at 30 °C. cAgNPs (a1 and b1), PVP-AgNPs (a2 and b2), CCM (a3 and b3).

Table 2
Minimal inhibitory concentrations of PVP-AgNPs, curcumin and their combinations against *E. coli* and *B. subtilis*.

Bacteria	(A) PVP-AgNPs		(B) CCM		FIC	Result
	MIC (only A) μg/mL	MIC (A in combination with B) μg/mL	MIC (only A) μg/mL	MIC (B in combination with A) μg/mL		
E. coli	32	8	64	8	0.375	Synergistic
B. subtilis	32	8	64	16	0.5	Synergistic

Note: Studies were done at 10^5 CFU ml^{-1} initial bacterial concentrations.

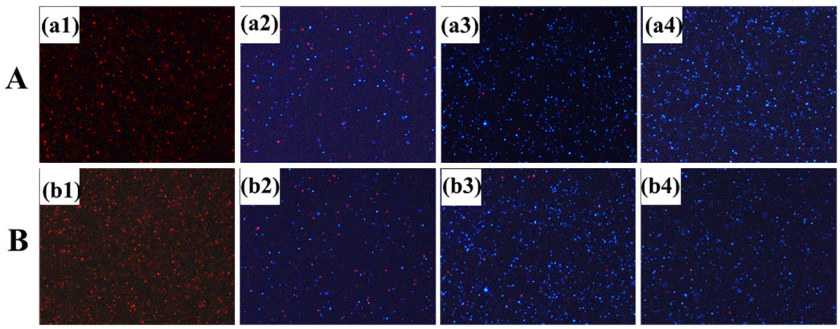

Fig. 4. Fluorescence microscope of *B. subtilis* (A) and *E. coli* (B). (a1, b1) stand for treated with cAgNPs, PVP-AgNPs (a2, b2), CCM (a3, b3) and control (a4, b4) after stained with PI and DAPI.

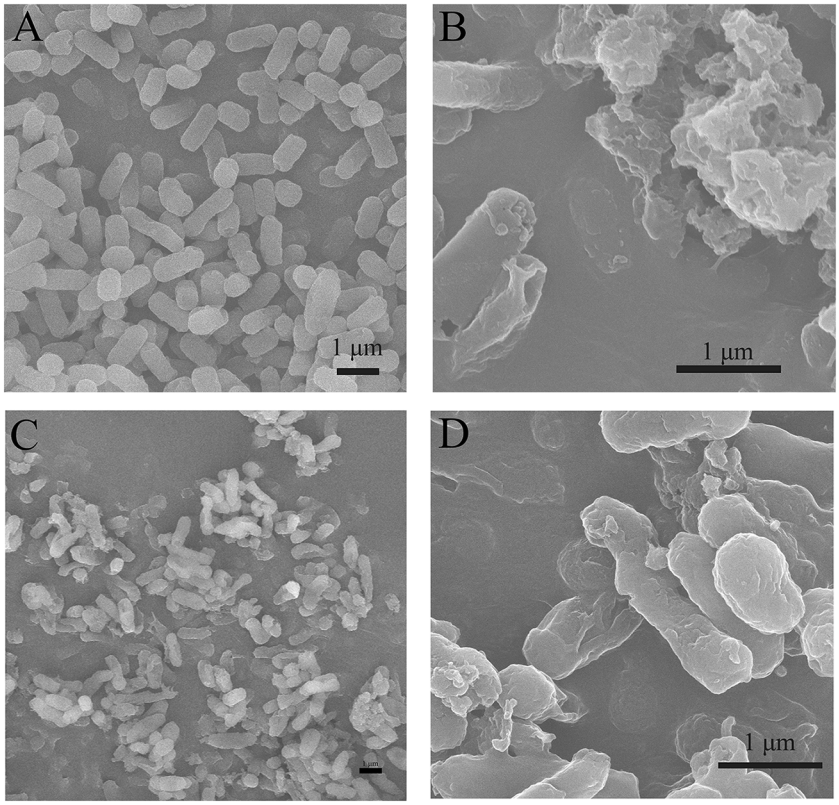

Fig. 5. SEM images of *B. subtilis* (A, B) and *E. coli* (C, D) after treatment with different conditions. A and C stand for no treatment bacterial, B and D stand for treated with cAgNPs.

3.3. Mechanism for synergistic antibacterial activity of combined AgNPs and curcumin

Previous studies demonstrate that nano-scaled silver have many different pathways of bactericidal activity, as discussed in several review papers [1,38]. They include the role of surface coating agents, uptake of free silver ions followed by disruption of ATP production and DNA replication, generation of reactive oxygen species, silver nanoparticle direct damage to cell membranes [39]. In our study, we propose a four–step pathway leading to the synergistic antibacterial activity: (1) curcumin act as a reducing agent and capping agent, form cAgNPs nanocomposites. (2) The cAgNPs nanocomposites bind to the bacterium and release Ag^+, more than PVP-AgNPs would release under the same conditions. (3) Generation of reactive oxygen species. (4) Membrane damage, bacterial lipases and induce leakage of intracellular contents followed by bacterial death.

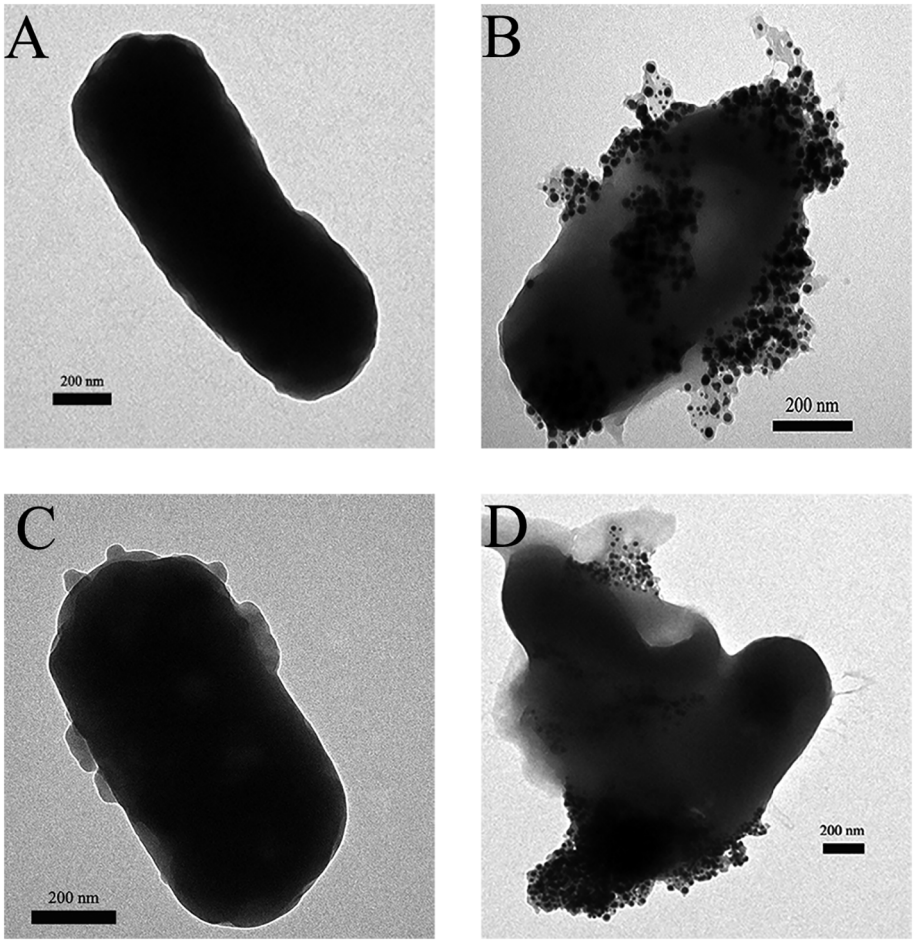

Fig. 6. TEM images of *B. subtilis* (A, B) and *E. coli* (C, D) after treatment with different conditions. A and C stand for no treatment bacterial, Band D stand for cAgNPs treatment.

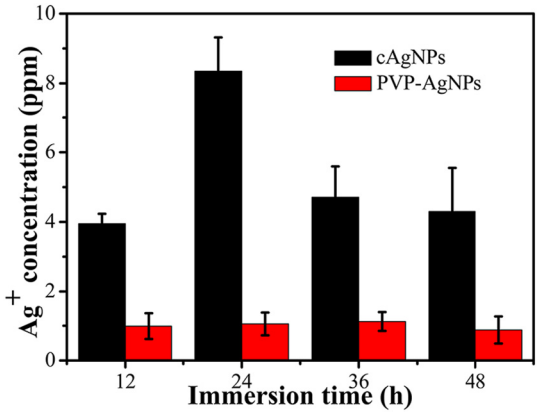

Fig. 7. Concentration of Ag^+ released from cAgNPs and PVP-AgNPs for different time treatment (12 h, 24 h, 36 h, 48 h).

3.3.1. Morphological

Morphological changes to *E. coli* and *B. subtilis* treated with cAgNPs were observed using scanning electron microscopy (SEM) and transmission electron microscopy (TEM). First, we carried out SEM experiments to test whether the integrity of bacterial cell walls can be disrupted by cAgNPs (Fig. 5). In the absence of cAgNPs nanocomposites, the shapes of *E. coli* and *B. subtilis* were typically rod-shaped and rounded, respectively. Both bacteria had globular morphology with smooth and intact cell walls. After incubation with cAgNPs nanocomposites, significant morphological changes to *E. coli* and *B. subtilis* could be observed compared to untreated-cells, treated bacteria cell walls were sunken and damaged, and the size and shape of the cells also changed dramatically, similar to previous reports [9,40,41]. Moreover, for most of the bacterial cells, leakage of intracellular contents could be tested as shown in the Fig. S3. Compared to the pure PVP-AgNPs and CCM treated group, the cAgNPs treated group show noticeable difference in the leakage of protein contents, indicating that cAgNPs treatment could disrupt the bacterial integrity and induce leakage of intracellular contents followed by bacterial death.

Similar phenomena were also observed in the cAgNPs treated cells of *B. subtilis* and *E. coli* by the TEM studies (Fig. 6). Following the silver ion treatment, the cytoplasm membrane shrank and cell wall was degraded. The cAgNPs treated bacterium group displayed a large number of nanoparticles on the bacterial surface, thus, it may create a temporary and local high Ag^+ concentration near the surface of the bacterium.

3.3.2. Ag^+ release

It has been reported that Ag^+ is the culprit for the antibacterial activity of AgNPs, while intact AgNPs may or may not directly induce toxicity [39]. It has also been reported that binding of AgNPs to the bacterial cells led to collapse of cell wall and bacterial death [42]. In this study, we examined Ag^+ release from AgNPs in the presence of the curcumin and PVP in cell culture medium to determine the effect of Ag^+ release on the inhibition of bacterial growth. Centrifugation (10,000 rpm) and filtration (0.22 μm) were used to separate intact AgNPs from the solution, leaving the Ag^+ in the supernatant solution. The released Ag^+ concentration and the corresponding percentage of

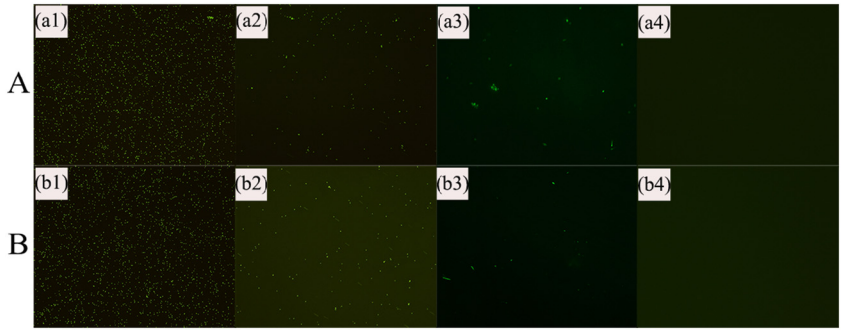

Fig. 8. ROS measurements of *B. subtilis* (A) and *E. coli* (B). Fluorescence microscope images treated with cAgNPs (a1, b1), PVP-AgNPs (a2, b2), CCM (a3, b3) and without treatment (a4, b4) after stained with DCFH-DA.

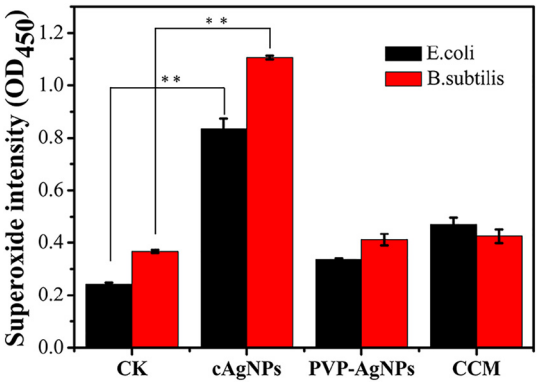

Fig. 9. Intracellular superoxide levels in the cAgNPs groups with comparison to control group (**P < 0.01).

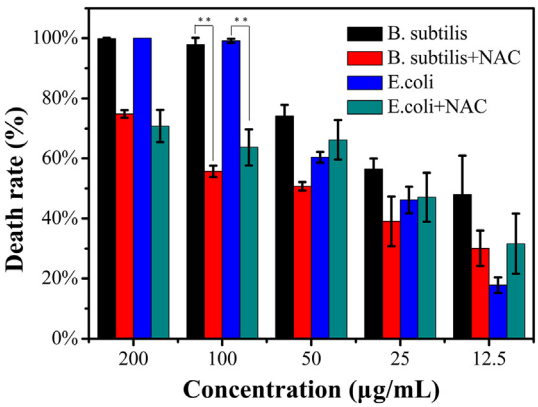

Fig. 10. The death rate of *B. subtilis* and *E. coli* bacterial added with NAC or not after treatment with different concentration of cAgNPs (**P < 0.01).

the total AgNP as shown in Fig. 7. The release rate of cAgNPs was increased of 4 to 8 folder than that of PVP-AgNPs and it reached the maximum at 24 h, however, the silver ion concentration of PVP-AgNPs was almost unchanged. This demonstrates that the presence of curcumin facilitates Ag^+ release. It has been demonstrated that silver nanoparticles can interact with the sulfur-containing proteins of cell walls and phosphorus containing compounds in cytoplasm, causing the function of cell respiration and cell division to be affected, resulting in the death of the bacteria [42]. Therefore, the Ag^+ release in the presence of bacterial cells is higher due to cellular binding. The further increase in Ag^+ release in the presence of curcumin signifies that the cAgNPs complex produces more Ag^+ and may cause more growth inhibition of the bacteria.

3.3.3. Intracellular ROS

Oxidative stress has been cited as one of the more important mechanisms of toxicity related to NPs exposure, they can damage DNA, cell membranes, and cellular proteins, and may lead to cell death [15]. To investigate the potential role of oxidative stress induced by cAgNPs, ROS generation in the presence of cAgNPs, PVP-AgNPs, CCM were monitored with oxidation-sensitive fluorescent probe DCFH-DA that passively diffuses through the cell membrane into the cell. The ROS level is in turn correlated with the antibacterial activity of the cAgNPs that is due to its damaging effect to the bacterial cell membrane. As shown in Fig. 8, when cultivated by the CCM or PVP-AgNPs, only a little the fluorescent signal was detected, while, a strong fluorescence signal was detected after treatment by cAgNPs. These results verify that cAgNPs induced intracellular ROS in bacteria and it should be responsible for the antibacterial effect.

The intracellular superoxide was quantitatively measured and the results shown in Fig. 9. OD450 reflects the intracellular superoxide level and cAgNPs treatment significantly increases the intracellular superoxide compare with PVP-AgNPs and CCM in *B. subtilis* and *E. coli* (P < 0.01).

To confirm the involvement of ROS in the antibacterial mechanism of cAgNPs, we evaluated the antibacterial activity of cAgNPs in the presence of *N*-acetyl-cysteine (NAC). The Fig. S4 shown that the death rate of cAgNPs was significantly decreased by in the presence of NAC. The results of the effect of NAC on the antibacterial activity of cAgNPs are shown in Fig. 10. The NAC test in its own that was used as the control, did not show any lethal effect on *E. coli* at the working concentration of 0.1 mM. cAgNPs alone showed strong antibacterial activity that killed 74.11% of the bacteria at a concentration of 50 μg/mL and killed almost 99% of the bacteria at 100 μg/mL. However, mortalities decreased to 50.7% and 55.6% when 0.1 mM NAC was added to AgNPs at 50 and 100 μg/mL, respectively. The similar results have also been got against the *E. coli*. These results demonstrated that the antibacterial activity of cAgNPs was attenuated in the presence of antioxidant (P < 0.01).

Taken together with the above results, it could be concluded that the enhanced antibacterial efficiency of cAgNPs was ascribed to increase ROS formation and the membrane damage followed by bacterial death.

4. Conclusion

In conclusion, efficient curcumin-modified silver nanoparticles were fabricated by a facile ultrasound treatment process. The cAgNPs solution has excellent characteristics such as monodisperse, homogeneous, biocompatible, and rapid release of silver ions. The cAgNPs not only solved the problem of curcumin is difficult to be absorbed, but also reflects the curcumin and silver nanoparticles of the two-common antibacterial effect. Compared with the conventional silver nanoparticles capped with PVP, the cAgNPs were possessed better antiviral

properties. The enhancement was the result of a synergistic effect between Ag nanoparticles and curcumin, our results demonstrated that the antibacterial mechanism of the cAgNPs nanocomposites attached to bacterial surface, thus, it creates a temporary and local high Ag^+ concentration near the surface of the bacterium, meanwhile, increase in Ag^+ release in the presence of curcumin, generation of more reactive oxygen species, lead to membrane damage, bacterial lipases and induce leakage of intracellular contents followed by bacterial death. More pharmacodynamics and toxicological studies of cAgNPs in appropriate animal models would be needed for future investigations. According to our results, cAgNPs might have potential to be developed as an effective antimicrobial nanomaterial.

Conflict and interest

The authors declare no competing financial interest.

Acknowledgement

The authors are grateful to the financial support by the National Natural Science Foundation of China (21375043, 21778020), the Fundamental Research Funds for the Central Universities (Grant No. 2662016QD027).

Appendix A. Supplementary data

Size and zeta potential of cAgNPs, content of Ag in the cAgNPs, bacteria membrane integrity evaluation, NAC or not after treatment with different concentration of cAgNPs. Supplementary data to this article can be found online at https://doi.org/10.1016/j.msec.2018.12.053.

References

[1] J.S. Kim, E. Kuk, K.N. Yu, J.H. Kim, S.J. Park, H.J. Lee, S.H. Kim, Y.K. Park, Y.H. Park, C.Y. Hwang, Y.K. Kim, Y.S. Lee, D.H. Jeong, M.H. Cho, Nanomedicine 3 (2007) 95–101.
[2] J.R. Morones, J.L. Elechiguerra, A. Camacho, K. Holt, J.B. Kouri, J.T. Ramirez, M.J. Yacaman, Nanotechnology 16 (2005) 2346–2353.
[3] J.N. Chen, L. Sun, Y. Cheng, Z.C. Lu, K. Shao, T.T. Li, C. Hu, H.Y. Han, ACS Appl. Mater. Interfaces 8 (2016) 24057–24070.
[4] W. Shao, X.F. Liu, H.H. Min, G.H. Dong, Q.Y. Feng, S.L. Zuo, ACS Appl. Mater. Interfaces 7 (2015) 6966–6973.
[5] M.M. Alves, O. Bouchami, A. Tavares, L. Cordoba, C.F. Santos, M. Miragaia, M.D. Montemor, ACS Appl. Mater. Interfaces 9 (2017) 28157–28167.
[6] Y.K. Qin, X.P. Guo, F.Y. Tou, H. Pan, J.N. Feng, J. Xu, B. Chen, M. Liu, Y. Yang, Environ. Sci. Nano 4 (2017) 1178–1188.
[7] H.Q. Feng, G.M. Wang, W.H. Jin, X.M. Zhang, Y.F. Huang, A. Gao, H. Wu, G.S. Wu, P.K. Chu, ACS Appl. Mater. Interfaces 8 (2016) 9662–9673.
[8] Y. Tao, E.G. Ju, J.S. Ren, X.G. Qu, Adv. Mater. 27 (2015) 1097–1104.
[9] Y.W. Wang, H. Tang, D. Wu, D. Liu, Y.F. Liu, A.N. Cao, H.F. Wang, Environ. Sci. Nano 3 (2016) 788–798.
[10] M. Rai, A. Yadav, A. Gade, Biotechnol. Adv. 27 (2009) 76–83.
[11] C.M. Zhao, W.X. Wang, Nanotoxicology 6 (2012) 361–370.
[12] O. Choi, Z.Q. Hu, Environ. Sci. Technol. 42 (2008) 4583–4588.
[13] J.S. McQuillan, H.G. Infante, E. Stokes, A.M. Shaw, Nanotoxicology 6 (2012) 857–866.
[14] J.C. Jin, Z.Q. Xu, P. Dong, L. Lai, J.Y. Lan, F.L. Jiang, Y. Liu, Carbon 94 (2015) 129–141.
[15] P.V. AshaRani, G. Low Kah Mun, M.P. Hande, S. Valiyaveettil, ACS Nano 3 (2009) 279–290.
[16] H.J. Yen, S.H. Hsu, C.L. Tsai, Small 5 (2009) 1553–1561.
[17] S. Pal, Y.K. Tak, J.M. Song, Appl. Environ. Microbiol. 73 (2007) 1712–1720.
[18] Y.J. Xiong, M. Brunson, J. Huh, A.R. Huang, A. Coster, K. Wendt, J. Fay, D. Qin, Small 9 (2013) 2628–2638.
[19] A.M. El Badawy, R.G. Silva, B. Morris, K.G. Scheckel, M.T. Suidan, T.M. Tolaymat, Environ. Sci. Technol. 45 (2011) 283–287.
[20] H.Y. Zhang, J.A. Smith, V. Oyanedel-Craver, Water Res. 46 (2012) 691–699.
[21] Y. Sun, Y. Xia, Science 298 (2002) 2176–2179.
[22] L. Maretti, P.S. Billone, Y. Liu, J.C. Scaiano, J. Am. Chem. Soc. 131 (2009) 13972–13980.
[23] S. Navaladian, B. Viswanathan, R.P. Viswanath, T.K. Varadarajan, Nanoscale Res. Lett. 2 (2007) 44–48.
[24] B.S. Yin, H.Y. Ma, S.Y. Wang, S.H. Chen, J. Phys. Chem. B 107 (2003) 8898–8904.
[25] M.N. Nadagouda, T.F. Speth, R.S. Varma, Acc. Chem. Res. 44 (2011) 469–478.
[26] J.R. Chiou, B.H. Lai, K.C. Hsu, D.H. Chen, J. Hazard. Mater. 248 (2013) 394–400.
[27] V. Dhand, L. Soumya, S. Bharadwaj, S. Chakra, D. Bhatt, B. Sreedhar, Mater. Sci. Eng. C Mater. Biol. Appl. 58 (2016) 36–43.
[28] W.J. Stark, Angew. Chem. Int. Ed. Eng. 50 (2011) 1242–1258.
[29] M. Poliakoff, J.M. Fitzpatrick, T.R. Farren, P.T. Anastas, Science 297 (2002) 807–810.
[30] S. Prasad, S.C. Gupta, A.K. Tyagi, B.B. Aggarwal, Biotechnol. Adv. 32 (2014) 1053–1064.
[31] S.Z. Moghadamtousi, H.A. Kadir, P. Hassandarvish, H. Tajik, S. Abubakar, K. Zandi, Biomed. Res. Int. (2014) 186864, , https://doi.org/10.1155/2014/186864.
[32] D. Sun, J.K. Zhou, L.S. Zhao, Z.Y. Zheng, J. Li, W.C. Pu, S.Y. Liu, X.S. Liu, S.J. Liu, Y. Zheng, Y. Zhao, Y. Peng, ACS Appl. Mater. Interfaces 9 (2017) 16858–16869.
[33] P. Anand, A.B. Kunnumakkara, R.A. Newman, B.B. Aggarwal, Mol. Pharm. 4 (2007) 807–818.
[34] U. Hani, H.G. Shivakumar, Curr. Drug Deliv. 11 (2014) 792–804.
[35] M. Taner, N. Sayar, I.G. Yulug, S. Suzer, J. Mater. Chem. 21 (2011) 13150–13154.
[36] H. Hanchi, R. Hammami, H. Gingras, R. Kourda, M.G. Bergeron, J.B. Hamida, M. Ouellette, I. Fliss, Future Microbiol 12 (2017) 205–212.
[37] S. Huo, Y. Jiang, A. Gupta, Z. Jiang, R.F. Landis, S. Hou, X.J. Liang, V.M. Rotello, ACS Nano 10 (2016) 8732–8737.
[38] M.J. Hajipour, K.M. Fromm, A.A. Ashkarran, D. Jimenez de Aberasturi, I.R. de Larramendi, T. Rojo, V. Serpooshan, W.J. Parak, M. Mahmoudi, Trends Biotechnol. 30 (2012) 499–511.
[39] H. Deng, D. McShan, Y. Zhang, S.S. Sinha, Z. Arslan, P.C. Ray, H.T. Yu, Environ. Sci. Technol. 50 (2016) 8840–8848.
[40] J.N. Chen, H. Peng, X.P. Wang, F. Shao, Z.D. Yuan, H.Y. Han, Nanoscale 6 (2014) 1879–1889.
[41] W.C. Hou, P.L. Lee, Y.C. Chou, Y.S. Wang, Environ. Sci. Nano 4 (2017) 647–657.
[42] W.K. Jung, H.C. Koo, K.W. Kim, S. Shin, S.H. Kim, Y.H. Park, Appl. Environ. Microbiol. 74 (2008) 2171–2178.